HHS Public Access

Author manuscript

Sci Transl Med. Author manuscript; available in PMC 2020 August 13.

Published in final edited form as:

Sci Transl Med. 2020 February 19; 12(531): . doi:10.1126/scitranslmed.aay4006.

A geometrically adaptable heart valve replacement

Sophie C. Hofferberth[1,*], **Mossab Y. Saeed**[1], **Lara Tomholt**[2,3], **Matheus C. Fernandes**[2,4], **Christopher J. Payne**[1], **Karl Price**[1], **Gerald R. Marx**[5], **Jesse J. Esch**[5], **David W. Brown**[5], **Jonathan Brown**[6], **Peter E. Hammer**[1], **Richard W. Bianco**[7], **James C. Weaver**[2], **Elazer R. Edelman**[6,8], **Pedro J. del Nido**[1,*]

[1]Department of Cardiac Surgery, Boston Children's Hospital, Harvard Medical School, Boston, MA 02115, USA

[2]Wyss Institute for Biologically Inspired Engineering, Harvard University, Cambridge, MA 02138, USA

[3]Harvard Graduate School of Design, Harvard University, Cambridge, MA, 02138, USA

[4]John A. Paulson School of Engineering and Applied Sciences, Harvard University, Cambridge, MA, 02138, USA

[5]Department of Cardiology, Boston Children's Hospital, Harvard Medical School, Boston, MA 02115, USA

[6]Biomedical Engineering Center, Institute for Medical Engineering & Science, Massachusetts Institute of Technology, Cambridge, MA 02139, USA

[7]Department of Surgery, University of Minnesota, Minneapolis, MN 55455, USA

[8]Cardiovascular Division, Department of Medicine, Brigham and Women's Hospital, Harvard Medical School, Boston, MA 02115, USA.

Abstract

Congenital heart valve disease has life-threatening consequences that warrant early valve replacement, however the development of a growth-accommodating prosthetic valve has remained elusive. Thousands of children continue to face multiple high-risk open-heart operations to replace valves that they have outgrown. Here, we demonstrate a biomimetic prosthetic valve that is

[*]Corresponding author. sophie.hofferberth@cardio.chboston.org (S.C.H.), pedro.delnido@cardio.chboston.org (P.J.d.N.).

Author contributions: S.C.H developed the concept, designed the valve, designed and performed the in vitro and in vivo experiments, analyzed the data, and wrote the manuscript. M.Y.S contributed to experimental design of acute in vivo studies and performed the valve implants. L.T generated the anatomical models and animations and contributed to manuscript preparation. M.C.F developed the finite element model for data analysis and contributed to manuscript preparation and editing. C.J.P contributed to valve design, CAD modeling, data analysis of acute in vivo experiments, and drafting of supplementary methods and figures. K.P contributed to CAD modeling and experimental design. G.R.M, J.J.E, D.W.B contributed to data analysis and performance of animal experiments. J.B contributed to the design of in vitro experiments. P.E.H contributed to experimental design and data analysis. R.W.B contributed to design of in vivo survival experiments and development of the growing lamb model. J.C.W coordinated 3D anatomical modeling and FEA studies and contributed to manuscript preparation. E.R.E contributed to experimental design, data analysis, manuscript preparation, and study oversight. P.J.d.N developed the project concept, contributed to experimental design, data analysis, manuscript editing and supervised the overall project. All authors read and edited the final version of the manuscript.

Competing Interests: S.C.H, P.J.d.N, E.R.E, P.E.H, C.J.P have a provisional patent application entitled "Geometrically-accommodating heart valve replacement device" (WO2019099864).

Data and materials availability: All data associated with this study are presented in the paper or the Supplementary Materials.

geometrically adaptable to accommodate somatic growth and structural asymmetries within the heart. Inspired by the human venous valve, whose geometry is optimized to preserve functionality across a wide range of constantly varying volume loads and diameters, our balloon-expandable synthetic bileaflet valve analog exhibits similar adaptability to dimensional and shape changes. Benchtop and acute in vivo experiments validated design functionality, and in vivo survival studies in growing sheep demonstrated that mechanical valve expansion accommodated growth. As illustrated in this work, dynamic size adaptability with preservation of unidirectional flow in prosthetic valves thus offers a paradigm-shift in the treatment of heart valve disease.

One-sentence summary:

A biomimetic prosthetic heart valve that is geometrically adaptable to accommodate somatic growth and structural asymmetries within the hearts of sheep.

INTRODUCTION

About 1.35 million children (°40,000 in the U.S) are born with a congenital heart defect each year worldwide (1). Indeed, the heart is the organ most commonly affected by birth malformations (2). In the U.S, an estimated 2.4 million children and adults are currently living with congenital heart disease (3), at an annual expense of ~$6 billion (4). Heart valve defects account for over 25% of all congenital heart disease (1, 5). Congenital malformations appear in all of the four native heart valves, including the semilunar pulmonary and aortic valves and the atrioventricular mitral and tricuspid valves, although the pulmonary valve is most often affected (1). Surgical intervention is usually required in the first few years of life to restore and maintain long term heart function. The primary goal of these procedures is to repair the native valve to allow for tissue growth, however this strategy is often not feasible or successful (6). As such, early valve replacement is inevitable in most children with congenital heart valve defects.

Outcomes of valve replacement remain suboptimal, particularly in young children, irrespective of whether biological cryopreserved human cadaveric donor valves, bioprosthetic tissue valves, or mechanical valves are placed. Biological valves exhibit accelerated structural deterioration from calcification and likely immune attack (7, 8), and mechanical valves bear added risk of life-long and life-threatening thromboembolic complications (9). Unfortunately, by design, all currently available prosthetic valves have a fixed functional diameter, and therefore cannot accommodate the growth of a child’s heart (10). Thus, children with congenital valvular defects face multiple invasive open-heart operations to upsize their fixed-size valve or valved conduit (11-13). Today, a child who undergoes valve replacement at less than two years of age will require up to five open-heart operations before reaching adulthood (14-16). Valve replacement surgery in children has serious associated morbidity, with inherent risk of stroke, rhythm abnormalities, bleeding complications, and prolonged hospital stay (12, 13, 16); moreover, mortality rates range from 2 to 30% (11, 12, 16).

Recently, stent-mounted tissue valves delivered via a transcatheter approach have emerged as a less invasive alternative for pulmonary valve replacement (17, 18). However, these

existing devices have limited expansion capacity and require large diameter delivery systems, which preclude valve implantation in infants and small children (19). Furthermore, valve deployment in older children and adolescents is often prohibited by large or asymmetric vessels (20). Many seek a growth-accommodating prosthetic valve, suitable for implantation from infancy through to adulthood. However, this is not a simple matter. Such a device must allow for annular circumference expansion, but without loss of function resulting from energy loss, stenoses, and/or regurgitation, or increased wear and tear.

Motivated by these requirements, here we demonstrate a biomimetic balloon-expandable prosthetic heart valve that is size-adjustable to accommodate somatic growth and compensate for structural asymmetries and dynamic structural oscillations. The valve design draws inspiration from the geometric profile of the native human venous valve, whose structure is optimized to preserve functionality in the face of marked vicissitudes in transmitted vascular volumes. We closely mimicked the dynamic structure-function relationship of the native venous valve to design a geometrically adaptable valve replacement device that maintains optimal function across a wide range of dimensions. We present the device concept, finite element computer simulation and flow-based in vitro analyses, acute in vivo studies evaluating function of the primary valve geometry, and in vivo survival studies demonstrating proof-of-concept of valve expansion in growing sheep.

RESULTS

Structure and function of human vascular valves

Although we traditionally associate valves with the heart, most valves within the body are vascular: only the atrioventricular valves are truly cardiac, containing myocardium and active contractile tissue structures. The semilunar arterial valves (Fig. 1A) are inherently passive and aside from needing to accommodate non-circular shape changes during the cardiac cycle, are relatively fixed in size. The semilunar valve leaflets insert into a fibrous annulus at attachment points (commissures) 120 degrees apart (Fig. 1B). The annulus is a semi-rigid ring of tissue that encircles the base of the valve and exhibits minimal change in diameter in loaded and unloaded states (21, 22). The aspect ratio of a semilunar valve is ~0.5:1, with an axial height about half the annulus diameter (Fig. 1B), and this is preserved throughout the cardiac cycle because the annulus dimension is relatively unchanged. As the annulus and leaflet dimensions increase with somatic growth (23), the aspect ratio is maintained (Fig. 1, B and C).

It is evident that the native semilunar valve geometry is not designed for dynamic diametric expansion. Our recent simulation-based study demonstrated non-living material with native semilunar valve geometry achieves <10% diameter increase before loss of valve function ensues (24). Since their introduction over half a century ago, bioprosthetic heart valves have traditionally mimicked the trileaflet semilunar valve geometry (25), and as such, all existing surgical prostheses are fixed in diameter. Even trileaflet balloon-expandable transcatheter valves have limited capacity for expansion beyond a single nominal diameter (26). Although the native semilunar valve design may be suitable for many adult patients, a non-living prosthesis with this geometry does not meet the physiologic and anatomic needs of a growing child.

In contrast to the arterial system, the venous system (Fig. 1D) not only returns blood to the heart, but also holds 70% of total blood volume and is 30-fold more compliant than arteries (27). As a capacitance reservoir, veins accommodate large changes in blood volume near-instantaneously (over a period of seconds) to maintain cardiac filling demands (27, 28) by modulating their circumferences, with up to a 4-fold change in vessel diameter (Fig. 1, E and F). Venous valves operate in this dynamic environment to ensure unidirectional flow with blood volume recruitment, and vessel diameter change without loss of valve competency (Fig. 1E). Unlike the semilunar valves, venous valve leaflets do not attach to a fibrous annulus. Rather, the two leaflets attach at the base of a bulbous sinus (the space between the valve leaflet and vein wall), located in a particularly thin region of the vein wall (Fig. 1E). The bulbous sinus expands radially outward under hydrostatic load, accounting for most of the vessel expansion at the level of the valve (29) (Fig. 1E). Moreover, venous valve leaflets are relatively non-compliant, exhibiting minimal change in surface area under load (30).

Early anatomic descriptions noted that the axial length of a human venous valve is about twice the vessel diameter (31), which we have also confirmed experimentally (Fig. 1E, fig. S1, table S1). Under resting conditions, in the closed position, venous valve leaflets coapt, contact each other, over a length corresponding to up to half the vessel diameter (32) (Fig. 1E). This coaptation reserve allows for continued leaflet contact under increasing volume loading. As the volume increases, the bulbous sinus dilates, pulling the leaflets radially outward, resulting in sac-like expansion along the valve base. Correspondingly, the valve aspect ratio and coaptation length decreases as the radial dimension increases (Fig. 1E, movie S1 - venous valve). The tall, bileaflet geometry, large leaflet surface area, and considerable coaptation reserve enable the venous valve to close effectively over a wide range of diameters to accommodate large changes in blood volume over short timescales (seconds, Fig. 1F) (33).

Biomimetic geometrically adaptable heart valve design

Drawing inspiration from the human venous valve, we explored the potential for a geometrically adaptable heart valve design. The fundamental geometric problem that must be overcome by a venous valve is identical to that for any prosthetic valve in a growing child: in both environments, the valve must maintain function while accommodating a diametrically expanding orifice. Throughout the course of this study, particular attention was paid to whether we could accommodate the dynamic and evolving dimensional changes imposed by growth by mimicking how the venous valve accounts for dynamic dimensional changes in transmitted ever-changing volumes (Fig. 2A).

The design of our biomimetic valve centers on three interrelated geometric components, including the leaflet profile geometry, the leaflet attachment geometry, and the valve expansion geometry. The leaflet profile geometry was created based on the morphology and dimensions observed in human venous valve specimens (fig. S1). Key dimensions included the valve axial length, baseline aspect ratio, leaflet mid-height, and leaflet free-edge length (Fig. 2A). The leaflet attachment geometry replicated the 3-dimensional geometric curve created by the venous valve leaflet attachment to the surrounding vessel wall (Fig. 1D, fig.

S1B, Fig. 2, fig. S2, movie S1-venous valve), and is the defining feature of the geometrically adaptable valve design. We developed a methodology for diametrically expanding the leaflet attachment geometry to achieve radial expansion. To accomplish this, we fixed the length of the 3-dimensional leaflet attachment perimeter such that radial expansion is accompanied by a reduction in valve height (Fig. 2A, fig. S3A). Thus, as the opening diameter increases, the valve shortens, thereby preserving coaptation without necessitating an increase in leaflet surface area (Fig. 2A).

Given the fixed length of the leaflet attachment perimeter, it is the baseline aspect ratio that determines the extent of functional valve expansion, and thereby the extent of growth-accommodation (fig. S3, B and C). Moreover, the baseline aspect ratio may be tailored based on the extent of desired expandability and anatomic constraints (figs. S3C, S4). By combining these critical biomimetic design components, we created a bileaflet valve with a dynamic geometric profile capable of adapting to the anatomic demands of a growing child via mechanical expansion (Fig. 2B).

In vitro characterization of primary biomimetic valve geometry

Benchtop testing examined how the varying aspect ratio of our stent design could achieve radial expansion without compromising valve function. We chose 0.1 mm expanded polytetrafluoroethylene (ePTFE) (Gore Preclude pericardial membrane, W.L Gore and Associates, Inc.) as the model leaflet material due to its limited compliance, ease of handling for prototyping purposes, proven clinical track record (34), and because its thin membrane and mechanical properties resemble the thin, inelastic native venous valve leaflet (29) (fig. S5). Using this material, we fabricated a series of valve prototypes at different states of diametric expansion, based on the proposed leaflet attachment and leaflet profile geometries (fig. S6). An in vitro circulatory flow loop system (fig. S7) was then used to define efficiency of forward flow and coaptation (closing function) across a range of expansion states (1X to 1.8X) (Fig. 3, A and B).

Using adjusted pressure and flow conditions to simulate the dynamic physiology of a growing child, we observed minimal pressure drop (Fig. 3A) and physiologic flow profiles (Fig. 3B, fig. S8) across all valve expansion states, thus demonstrating that the biomimetic valve design enables unobstructed forward flow over a wide range of vessel sizes and flow rates. As expected, leaflet deformation in the closed state depended on the degree of expansion and pressure, but not at the expense of coaptation. Coaptation under dynamic right and left heart loading conditions well exceeded industry standards (ISO 5840-2:2015) across all valve expansion geometries (Fig. 3C). Valve closing function was not dependent on cycle rate, demonstrating that this leaflet geometry does not display inertial effects, which theoretically could inhibit valve closure in hyperdynamic physiological states, such as in a young child with a rapid heart rate.

To understand leaflet deformation and its stress distribution, we constructed a finite element (FE) model of the expanding valve leaflet in a quasi-static loaded state, under right (Fig. 3D, fig. S9) and left heart diastolic loading conditions (fig. S9). Maximum leaflet stresses were at least a factor of 30 below the failure stress of 0.1 mm ePTFE (Goretex) for all valve expansion states and loading conditions. We also repeated the same analysis at smaller,

pediatric-specific valve sizes, and found that the highest stress values were further reduced by >40% (fig. S10). There were no areas of stress concentration along the leaflet-frame interface, or elsewhere across the leaflet surface. The lowest stress regions were located at the leaflet commissures (where leaflets meet and insert into the frame) and along the leaflet free edge (region of leaflet contact) (Fig. 3D). The pattern of stress distribution is important for the life cycle of a heart valve device, because the presence of localized, high stress regions in trileaflet bioprosthetic valves has been associated with early device failure (35, 36). Furthermore, compression and bending of redundant tissue in trileaflet designs leads to alternating negative and positive stress values, which likely induces earlier valve deterioration (35, 37, 38). This pattern was not observed in the bileaflet valve geometry (Fig. 3D, fig. S9).

In vivo validation of primary biomimetic valve geometry

To validate valve performance in an in vivo environment, an acute large animal model was established using the two polar expansion states (1X and 1.8X). To match the state of valve expansion to the relevant physiologic environment, fabricated prototypes were implanted in the native pulmonary valve position of juvenile (1X geometry, N = 4) and adult (1.8X geometry, N = 4) sheep (Fig. 4, A and B). Valves were implanted using standard surgical techniques, and the animals were observed for 4 - 6 hours. In all animals, using both geometric configurations, valve hemodynamic performance remained ideal, with trivial transvalvular gradient (pressure drop) (Figs. 4, C and D, fig. S11, tables S2, S3) and physiologic flow profiles (Figs. 4, E and F, fig. S11). Color Doppler images obtained via epicardial echocardiogram demonstrated laminar flow along the length of the valve and into the branch pulmonary arteries (movie S1 - Primary biomimetic valve geometry). Valve coaptation was effective, with no clinically relevant leakage (Fig 4, E and F) observed in any of the eight animal studies (fig. S11, tables S4, S5). Representative echocardiographic imaging (Fig. 4, G and H, movie S1 - Primary biomimetic valve geometry) confirmed these observations and the change in leaflet coaptation length from baseline to complete expansion. For proof-of-principle, the biomimetic valve was implanted in the native aortic valve position of juvenile sheep, demonstrating equivalent mechanical and hemodynamic performance, with unobstructed forward flow and preserved leaflet coaptation at each stage of valve expansion (fig. S12).

These experiments validated our benchtop results and demonstrated proof-of-concept in vivo. The consistency of valve function over a wide range of hemodynamic conditions and expansion states highlights the versatility of the biomimetic bileaflet valve design. The kinematic profile of the leaflet attachment geometry is crucial to valve adaptability, since the decrease in valve height with radial expansion preserves the U-shaped geometry of the leaflet free edge (Fig. 2B), which serves to retain optimal leaflet mobility across all expansion states (movie S1 - primary biomimetic valve expansion). Preserved leaflet mobility thus enables the effective orifice area to increase commensurate with valve diameter and obviates the risk of flow stasis at the valve base.

In vitro design and validation of the expandable biomimetic valve prototype and in vivo proof-of concept in growing lambs

To construct a mechanically-expandable biomimetic valve prototype, circumferential restraining struts were added to optimize structural support and the kinematic profile of the leaflet attachment geometry, while maintaining device symmetry and concentricity (Fig. 5, A to D). The geometry, path length, and, critically, the location of these support features may be modulated to achieve a circular, out-of-round, or asymmetric expansion profile.

Prototypes were fabricated from 0.1 mm thickness ePTFE leaflets hand-sewn to a laser-cut stainless-steel stent (fig. S13). Valves were tested in an in vitro circulatory flow loop system (fig. S7), under simulated pediatric-specific hydrodynamic conditions (ISO 5840-2:2015). Akin to the primary valve geometry, the expandable prototype displayed excellent forward flow efficiency (Fig. 5e, fig. S14), with trivial pressure drop (fig. S14) and a >4-fold increase in effective orifice area from 1X to 1.8X diameter expansion (fig. S14). The indexed effective orifice area (valve diameter/body surface area) increased with progressive valve expansion from 1X to 1.8X (fig. S14), thus indicating that the area of valve opening was preserved along the full length of the leaflet, from the proximal valve opening to the distal leaflet free edge. This geometric feature enables the expandable biomimetic bileaflet valve to maintain optimal forward flow across a wide range of diameters. Moreover, the expandable prototype design maintained effective coaptation along the full length of the leaflet free edge across all expansion states (1X to 1.8X), under both right and left heart diastolic loads (Fig. 5e, S14).

Motivated by these benchtop results, we next investigated proof-of-concept in vivo mechanical device expansion during somatic growth in lambs. Expandable biomimetic valve prototypes were implanted in the native pulmonary valve position of seven juvenile sheep (mean weight = 22.5 ± 0.9 kg, mean age = 9 ± 3 weeks). Implanted valves were expanded via transcatheter balloon dilation at three separate time points over a 9-10 week survival period. The animals received subcutaneous heparin twice daily for five days after valve implantation, and for two days after each balloon expansion. There was no chronic anticoagulant or antiplatelet therapy administered. Lambs displayed expected growth profiles, gaining >60% in body weight (mean weight at term = 36.7 ± 3.5kg), and their prosthetic valves achieved a 1.6X [20 mm internal diameter (ID)] diametric expansion (Fig. 5F). In all animals, valve expansions were atraumatic, uniform, and symmetric (Fig. 5E, F), and there was no measurable elastic recoil of the frame after dilation.

Kinematics of the leaflet attachment geometry over 2.5 months of in vivo implantation and multiple balloon dilations (Fig. 5F) mirrored what was modeled computationally and observed in our benchtop experiments (Fig. 3, fig. S13). Leaflet mobility and coaptation were preserved to achieve unidirectional pulmonary blood flow at all expansion states [movie S1-representative two-dimensional (2D) echocardiogram color Doppler images]. Forward flow efficiency was maintained as the expanding valve orifice matched the hemodynamic demands of the growing lamb (Fig. 5G, table S6, S7). Cardiac catheterization demonstrated intact right ventricular function, low transvalvular pressure gradients, and a commensurate increase in cardiac output as the valve was expanded up to 1.6X diameter. Serial 2D transthoracic echocardiogram with continuous wave Doppler demonstrated

parabolic flow profiles, with low transvalvular flow velocity at each stage of valve expansion from 12.5 mm to 20 mm ID (fig. S15). This data highlights the absence of functional stenosis with valve diametric expansion. Comprehensive hemodynamic data are presented in tables S6 and S7. At term, six of the seven animals showed no evidence of valve regurgitation, and one animal had trivial to mild regurgitation, based on angiographic and echocardiographic imaging movie S1 - Expandable biomimetic valve geometry, fig. S15).

Necropsy and histopathological analysis demonstrated minimal tissue inflammation, healthy right ventricular muscle, and no evidence of distal thrombo-emboli (Fig. 6, fig. S16). In all study animals, the pulmonary artery wall exhibited no evidence of vessel injury after chronic implantation and three transcatheter balloon expansions. There was only minimal compression of the underlying intimal and medial layers in the regions of stent contact (Fig. 6, C to E, fig. S17). The ePTFE sewing cuff on the valve exterior exhibited a normal fibrocellular tissue healing response and minimal inflammatory cell infiltrate (Fig. 6. C, F, G) in all animals. The inflow and outflow surfaces of all explanted valves had minimal tissue ingrowth and were free of thrombus (blood clots). The 0.1 mm ePTFE leaflets remained intact, thin, and pliable, with minimal surface irregularities and no evidence of microfractures (Figs. 6, C, F to H, fig. S16, fig. S17). There was no inflammatory cell infiltrate and no clinically relevant thrombus present in any of the seven explanted valve specimens (Fig. 6, figs. S16, S17).

This proof-of-concept survival study demonstrated the safety and feasibility of valve balloon expansion to accommodate somatic growth. Preserved leaflet function and the lack of thrombus formation, in the absence of chronic anticoagulant therapy, suggests that the biomimetic bileaflet valve geometry has favorable perivalvular flow dynamics, facilitating effective sinus washout and minimizing flow stagnation across all expansion states (movie S1 - term echocardiograms, color flow profile). This flow pattern appears similar to native venous valves, where flow separation and formation of large-scale vortices behind the valve leaflets prevents stasis in the sinus pockets (39, 40). As such, the fluid mechanics demonstrated in this valve design will be an important determinant of long-term device durability.

DISCUSSION

Here, we introduce a biomimetic bileaflet prosthetic valve that is balloon-expandable to accommodate somatic growth and structural asymmetries within the heart, without loss of functional integrity. Benchtop and acute in vivo experiments validated functional performance and computational modeling demonstrated a favorable stress-strain profile under physiological loads, suggesting a potentially durable valve design. In vivo survival studies of 9-10 weeks duration in growing lambs demonstrated successful valve balloon expansion to accommodate growth. Commercially available, non-expansile materials enabled diametric expansion without requiring redundant leaflet surface area, thus demonstrating the compatibility of this design with a variety of synthetic and tissue leaflet materials.

A growth-accommodating prosthetic heart valve would greatly advance pediatric cardiovascular medicine, since each year over 330,000 children are born with a congenital valve defect worldwide (1). Moreover, acquired rheumatic heart disease affects over 5 million school-age children worldwide, many of whom require early valve replacement (41). Thus, existing fixed-size prostheses leave hundreds of thousands of children at risk for multiple, invasive open-heart procedures over their lifetime. Moreover, valve replacement is often delayed due to size limitations of current devices, further compounding serious morbidity. In contrast, our valve design accommodates child growth, and its adjustable dimensions enable implantation at any age. As a result, infants and children could potentially reach adulthood after receiving one valve implant. Such a technological breakthrough would avoid multiple surgeries, reducing lifetime morbidity and mortality and healthcare costs, as each valve replacement procedure alone costs ~$50,000 (42).

We envision clinical application as in our growing animal model, in which valve implantation is performed as soon as clinically indicated, followed by periodic valve expansion via a minimally invasive transcatheter approach. Patient populations facing loss of native valve function in the first few years of life would stand to benefit from successful clinical translation of this technology. One such example is tetralogy of Fallot - the most common congenital right heart defect, accounting for ~130,000 live births per year worldwide (1). The serious morbidity of this defect necessitates surgical correction within the first year of life, however, current approaches fail to preserve pulmonary valve function, leading to progressive right ventricular dilation, and subsequent risk of exercise intolerance, ventricular dysfunction, and life-threatening arrhythmias as these patients approach adulthood (43-45). To avoid these deleterious long-term outcomes, pulmonary valve replacement is performed, usually in the second decade of life. Unfortunately, the adverse effects of chronic valve insufficiency are often irreversible. Moreover, these children face repeated interventions to replace valves they have outgrown. Thus, a pulmonary valve replacement that is implantable during infancy and functions through to adulthood would represent a paradigm-shifting advance in the care of children with tetralogy of Fallot. We envision the timing of interventions and extent of valve expansion would be customized based on the individual child’s hemodynamic and growth status.

A geometrically versatile bileaflet valve design has promise in adults as well, particularly for those with small annuli, irregular valve geometry, or intermediate valve dimensions, which predispose to suboptimal procedural outcomes (46, 47). The ability to expand and function in non-circular, asymmetric environments may also accommodate adults with extreme annular eccentricity (48, 49), native bicuspid anatomy (50), and those with predominant aortic regurgitation (51). Further work is required to enable transcatheter deployment of this device, however the biomimetic geometrically adaptable valve design has potential to expand the indications for transcatheter valve implantation to patient subgroups currently not served by existing technology.

We successfully demonstrated proof of concept for the expandable biomimetic valve, but we acknowledge this study has limitations, and that further work is required to advance this technology towards clinical translation. First, longer-term animal studies are required to assess the chronic effects of valve implantation, including vessel remodeling and growth,

thrombosis, and leaflet degeneration/calcification in response to multiple valve dilations. Moreover, long-term in vivo studies are needed to evaluate how flow mechanics generated by the bileaflet valve geometry influence vascular remodeling. Second, benchtop durability testing will be required to characterize structural integrity of the expandable biomimetic valve prototype. Third, although we used 0.1 mm ePTFE as the model leaflet material in this study, further work is required to determine whether this is the optimal material for clinical applications. Other substitute leaflet materials should be tested within the geometrically adaptable stent design. Fourth, stress and fatigue life analyses of the expandable stent design, including external compression testing, are necessary to identify potential failure modes and optimize frame geometry. Finally, once the optimal design is identified, we will need to explore advanced manufacturing and materials processing techniques to assemble a valve prototype for pre-clinical and, ultimately, clinical testing.

In conclusion, we demonstrate the advantage and potential of a balloon-expandable geometrically adaptable heart valve prosthesis that recapitulates the natural dimension-dynamic operation of venous valves. Mimicking natural venous valve design, we present a bileaflet valve design of programmed dimensions and aspect ratio that adapts to growth without loss of unidirectional flow control. Controlled local fluid dynamics minimizes thrombotic, tissue hyperplastic and flow disruptions that restrict the use of current valve devices. Incorporation of these geometrically adaptable functionalities thus offers the potential for a paradigm-shift in the treatment of pediatric and adult heart valve defects.

MATERIALS AND METHODS

Study design

The objective of this study was to design a size-adjustable prosthetic heart valve that functions optimally over a wide range of dimensions. Physical prototyping using additive manufacturing techniques, finite element modeling, in vitro hydrodynamic performance testing, x-ray imaging, and benchtop fabrication were utilized to optimize device design. To demonstrate functional performance of the primary biomimetic valve geometry, we initially tested the device in an in vivo, non-survival ovine model. The device was implanted in the native pulmonary valve position of juvenile and adult sheep at two polar states of valve expansion; i) a 1X geometry (14 mm ID) valve prototype was implanted in N = 4 lambs (weight: 20 kg) and ii) a 1.8X geometry (25 mm ID) valve prototype was implanted in N = 4 adult sheep (weight: 60 kg). Animals were observed for 4-6 hours post valve implantation. Valve hemodynamic performance was assessed via continuous measurement of transvalvular pressure gradient and main pulmonary artery flow. Valve mechanical performance was evaluated via 2D and 3D epicardial echocardiography, performed serially during the observation period. To demonstrate proof-of-concept of our biomimetic expandable valve design, we established a preclinical in vivo growing lamb model. This single-arm study was not blinded or randomized. Seven lambs (aged 6 to 15 weeks) underwent surgical implantation of a 12.5 mm ID expandable biomimetic valve prototype in the native pulmonary valve position. To accommodate somatic growth of the animal, the valve was expanded via serial transcatheter balloon dilation procedures performed at 2-, 6- and 8-weeks post-implantation. Each animal reached an expanded valve diameter of 20 mm ID

(1.6X expansion). The survival period ranged from 9 to 10 weeks. Valve hemodynamic performance and heart function were investigated via serial intracardiac catheterization, angiography, and 2-D transthoracic and epicardial echocardiography. After a minimum of 63 days (range, 63 - 68 days), the valves were explanted and assessed macroscopically and histologically.

Valve prototype design and material selection

Creation, design, and material selection for the venous valve-inspired bileaflet valve is described in the Supplementary Materials. We studied the morphology and dimensions of human venous valve specimens (n = 4) and used these geometric design inputs to generate the biomimetic bileaflet valve geometry. To determine optimal valve length for growth accommodation, we measured the critical anatomic dimensions of the youngest pediatric patients who require heart valve replacement. We performed biaxial mechanical testing of select leaflet materials under physiologic valve loading conditions and chose a leaflet material with limited compliance to mimic the mechanical properties of native human venous valves (0.1 mm ePTFE).

Fabrication

All fabrication processes are described in detail in the Supplementary Materials. Physical prototypes of the primary biomimetic valve geometry were additively manufactured from cobalt chromium using direct metal laser sintering. Leaflets were cut from 0.1mm ePTFE (Gore Preclude pericardial membrane, W. L. Gore & Associates) and were sewn into the leaflet attachment frame. The expandable biomimetic valve prototype was fabricated from 0.1 mm ePTFE leaflets sewn into a laser-cut stainless steel (316L) stent (Resonetics Israel Ltd).

In vitro testing

In vitro hydrodynamic performance testing—Valve prototypes were tested in an in vitro pulsatile flow loop apparatus (ViVitro Labs Inc, Victoria, BC Canada). The in vitro circulatory flow loop set up is illustrated in Fig. S7. A comprehensive series of hydrodynamic experiments were performed to characterize transvalvular pressure gradient (pressure drop), effective orifice area, and valve coaptation (competence) over a wide range of physiologic and supraphysiologic flow and pressure conditions. A mixture of 0.9 ± 0.2% sodium chloride in glycerin and distilled water was used as the working fluid to emulate blood properties.

Finite Element modeling—We performed a Finite Element (FE) analysis of the biomimetic bileaflet valve. Construction and processing of the FE model is described in detail in the Supplementary Materials. Briefly, a FE model was constructed to evaluate the magnitude and distribution of stresses on the biomimetic valve leaflet in a quasi-static, closed position (diastolic phase of the cardiac cycle). The leaflet-stent model was constructed using the commercial Computer Aided Design (CAD) software SolidWorks (Dassault Systèmes). The FE simulations were performed using the commercial solver ABAQUS/Explicit 2017 (Dassault Systèmes).

In vivo acute ovine studies

Acute in vivo studies were conducted in juvenile sheep to evaluate functional performance of the primary biomimetic valve geometry, at two polar expansion states (1X-14 mm ID, 1.8X-25 mm ID). All animal experiments were conducted in full compliance with the 1996 Guide for the Care and Use of Laboratory Animals recommended by the U.S. National Institutes of Health. The acute in vivo studies were performed at Boston Children's Hospital and the experimental protocol was approved by the hospital's Institutional Animal Care and Use Committee. Female Dorset lambs (N = 8, Parsons EM and Sons Inc) with a body weight of 20 kg (1X geometry, N = 4) and 60 kg (1.8X geometry, N = 4) were used. Anesthesia induction and maintenance are described in the Supplementary Materials. A left-sided thoracotomy was performed to access the chest for valve implantation and instrumentation. Transvalvular pressure gradient was evaluated via placement of right ventricular and pulmonary artery pressure lines and cardiac output was measured via perivascular flow probe (Transonics, TS420) placement around the main pulmonary artery. Epicardial echocardiographic imaging was performed to obtain native pulmonary valve and main pulmonary artery dimensions and assess overall heart function. After being heparinized (300 IU/kg), animals were cannulated for cardiopulmonary bypass. With animals cooled to 33°C and under beating heart conditions, valve prototypes were implanted in the native pulmonary valve position. Details of the surgical technique are described in the Supplementary Materials. Animals were weaned off cardiopulmonary bypass post device implantation and observed for 4 to 6 hours. 2-D epicardial echocardiography, including color and continuous wave Doppler imaging, and 3-D echocardiography were performed at multiple timepoints by a cardiologist who specializes in echocardiographic imaging. Continuous monitoring of right ventricular and pulmonary artery pressures, and main pulmonary artery flow were performed. All data were logged continuously in real time using a LabChart data logger (AD instruments). At the conclusion of the study, animals were euthanized by intravenous injection of overdosed pentobarbital sodium (Fatal-Plus, 86 mg/kg). The heart was excised and opened for direct inspection of the valve.

In vivo survival ovine studies

In vivo survival studies in growing lambs were performed to demonstrate proof-of-concept of valve expansion. All survival implants were conducted at the University of Minnesota, Experimental Surgical Services animal facility. Experiments were conducted in compliance with the National Institutes of Health (NIH) Guide for the Care and Use of Laboratory Animals. The experimental protocol was approved by the University of Minnesota's Institutional Animal Care and Use Committee. Male and non-pregnant female Polypay and Hampshire breed juvenile sheep were used (N = 7, weight 22-24kg). Animal preparation, anesthesia induction and maintenance, and details of the surgical procedure are described in the Supplementary Materials. Briefly, a left thoracotomy was performed, animals were cannulated for cardiopulmonary bypass and the expandable biomimetic valve prototype was implanted in the native pulmonary valve position (See Supplementary Materials). After implantation and wean from cardiopulmonary bypass, Protamine was administered for heparin reversal. 2-D epicardial echocardiography was performed to evaluate device performance and overall heart function. Post-operatively, animals received subcutaneous Heparin (1000 IU) once the evening of surgery and then twice daily for 5 days.

To accommodate somatic growth, animals underwent transcatheter balloon dilation of the valve implant at three separate timepoints during the survival period (2-, 6-, and 8 weeks post implant). Details of the valve expansion experimental protocol are outlined in the Supplementary Materials. Briefly, a 14Fr introducer sheath was placed in the right jugular vein. Intravenous heparin (250 mg/kg) was administered and a Swan-Ganz catheter was inserted to measure transvalvular pressure gradient and cardiac output prior to valve dilation. Right ventricular and main pulmonary artery angiography was performed via injection of contrast and visualization under fluoroscopy. A guide wire was then introduced and an appropriately sized percutaneous balloon catheter (Atlas PTA Balloon Dilation Catheter) was advanced into position across the valve device. Under direct fluoroscopic visualization, the balloon was inflated to a nominal pressure of 6 atm to expand the valve. Valve performance and heart function were assessed post-dilation via right ventricular and main pulmonary artery angiogram and repeat measurement of transvalvular pressure gradient and cardiac output. After each valve dilation, animals received one dose of subcutaneous Heparin (1000 IU) the evening of the procedure and twice daily administration for 2 days.

Interval transthoracic echocardiography was performed to assess valve performance and heart function in the week prior to and following each scheduled balloon dilation procedure. At term, animals were anesthetized and intracardiac hemodynamic measurements and angiographic imaging were obtained. A right thoracotomy incision exposed the heart and 2-D epicardial echocardiography was performed to assess device performance and overall heart function. Animals were euthanized by intravenous injection of phenytoin/pentobarbital solution. Necropsy was performed, with examination of the heart and valve implant. Gross pathological findings were also examined in the kidneys, lungs, brain, liver, spleen and gastrointestinal tract.

Explanted valves and attached pulmonary artery tissue were fixed in formalin and sent for plastic embedding and sectioning. Tissue samples were stained with H&E and Miller’s elastic stain and examined using brightfield optical microscopy. Four representative sections were examined per animal.

Statistical analysis

Hemodynamic data were analyzed using LabChart (AD Instruments). Methods of quantifying valve regurgitant volumes and transvalvular pressure gradients are described in the Supplementary Materials. Ten representative cycles for each condition were analyzed. Pulmonary artery flow, right ventricular and pulmonary artery pressures values were obtained by recording at 0.005 second intervals and then averaging the values for each over 10 consecutive cardiac cycles. Standard deviations are representative of cycle-to-cycle variations.

Supplementary Material

Refer to Web version on PubMed Central for supplementary material.

ACKNOWLEDGEMENTS

We thank J. Carney and the UMN Experimental Surgical Services lab for help with design of the survival animal studies and for conducting the experiments; J. E. Mayer for surgical expertise and helpful discussions; C. W. Baird for helpful discussions; and O. Barry and B. Quinn for technical support with animal procedures.

Funding: S.C.H was supported by a National Institutes of Health - NRSA post-doctoral fellowship grant (1F32HL138993-01) and an Early Career Award from the Thrasher Research Fund. This project was supported by the Oakwood Foundation.

REFERENCES AND NOTES

1. van der Linde D, Konings EE, Slager MA, Witsenburg M, Helbing WA, Takkenberg JJ, Roos-Hesselink JW, Birth prevalence of congenital heart disease worldwide: a systematic review and meta-analysis. J Am Coll Cardiol 58, 2241–2247 (2011). [PubMed: 22078432]
2. Bernier PL, Stefanescu A, Samoukovic G, Tchervenkov CI, The challenge of congenital heart disease worldwide: epidemiologic and demographic facts. Semin Thorac Cardiovasc Surg Pediatr Card Surg Annu 13, 26–34 (2010). [PubMed: 20307858]
3. Gilboa SM, Devine OJ, Kucik JE, Oster ME, Riehle-Colarusso T, Nembhard WN, Xu P, Correa A, Jenkins K, Marelli AJ, Congenital Heart Defects in the United States: Estimating the Magnitude of the Affected Population in 2010. Circulation 134, 101–109 (2016). [PubMed: 27382105]
4. Benjamin EJ, Blaha MJ, Chiuve SE, Cushman M, Das SR, Deo R, de Ferranti SD, Floyd J, Fornage M, Gillespie C, Isasi CR, Jimenez MC, Jordan LC, Judd SE, Lackland D, Lichtman JH, Lisabeth L, Liu S, Longenecker CT, Mackey RH, Matsushita K, Mozaffarian D, Mussolino ME, Nasir K, Neumar RW, Palaniappan L, Pandey DK, Thiagarajan RR, Reeves MJ, Ritchey M, Rodriguez CJ, Roth GA, Rosamond WD, Sasson C, Towfighi A, Tsao CW, Turner MB, Virani SS, Voeks JH, Willey JZ, Wilkins JT, Wu JH, Alger HM, Wong SS, Muntner P, American C Heart Association Statistics, S. Stroke Statistics, Heart Disease and Stroke Statistics-2017 Update: A Report From the American Heart Association. Circulation 135, e146–e603 (2017). [PubMed: 28122885]
5. Hoffman J, The global burden of congenital heart disease. Cardiovasc J Afr 24, 141–145 (2013). [PubMed: 24217047]
6. Husain SA, Brown JW, When reconstruction fails or is not feasible: valve replacement options in the pediatric population. Semin Thorac Cardiovasc Surg Pediatr Card Surg Annu, 117–124 (2007). [PubMed: 17434003]
7. Chen PC, Sager MS, Zurakowski D, Pigula FA, Baird CW, Mayer JE Jr., Del Nido PJ, Emani SM, Younger age and valve oversizing are predictors of structural valve deterioration after pulmonary valve replacement in patients with tetralogy of Fallot. J Thorac Cardiovasc Surg 143, 352–360 (2012). [PubMed: 22153723]
8. Karamlou T, Blackstone EH, Hawkins JA, Jacobs ML, Kanter KR, Brown JW, Mavroudis C, Caldarone CA, Williams WG, McCrindle BW, Pulmonary S Conduit Working Group for the members of the Congenital Heart Surgeons, Can pulmonary conduit dysfunction and failure be reduced in infants and children less than age 2 years at initial implantation? J Thorac Cardiovasc Surg 132, 829–838 (2006). [PubMed: 17000294]
9. Lubiszewska B, Rozanski J, Szufladowicz M, Szaroszyk W, Hoffman P, Ksiezycka E, Rydlewska-Sadowska W, Ruzyllo W, Mechanical valve replacement in congenital heart disease in children. J Heart Valve Dis 8, 74–79 (1999). [PubMed: 10096487]
10. Henaine R, Roubertie F, Vergnat M, Ninet J, Valve replacement in children: a challenge for a whole life. Arch Cardiovasc Dis 105, 517–528 (2012). [PubMed: 23062483]
11. Alsoufi B, Manlhiot C, Al-Ahmadi M, McCrindle BW, Kalloghlian A, Siblini G, Bulbul Z, Al-Halees Z, Outcomes and associated risk factors for mitral valve replacement in children. Eur J Cardiothorac Surg 40, 543–551 (2011). [PubMed: 21353791]
12. Karamlou T, Jang K, Williams WG, Caldarone CA, Van Arsdell G, Coles JG, McCrindle BW, Outcomes and associated risk factors for aortic valve replacement in 160 children: a competing-risks analysis. Circulation 112, 3462–3469 (2005). [PubMed: 16316968]

13. Nomoto R, Sleeper LA, Borisuk MJ, Bergerson L, Pigula FA, Emani S, Fynn-Thompson F, Mayer JE, Del Nido PJ, Baird CW, Outcome and performance of bioprosthetic pulmonary valve replacement in patients with congenital heart disease. J Thorac Cardiovasc Surg 152, 1333–1342 e1333 (2016). [PubMed: 27637422]
14. Kanter KR, Forbess JM, Kirshbom PM, Redo mitral valve replacement in children. Ann Thorac Surg 80, 642–645; discussion 645-646 (2005). [PubMed: 16039220]
15. Kanter KR, Kirshbom PM, Kogon BE, Redo aortic valve replacement in children. Ann Thorac Surg 82, 1594–1597 (2006). [PubMed: 17062211]
16. Woods RK, Pasquali SK, Jacobs ML, Austin EH, Jacobs JP, Krolikowski M, Mitchell ME, Pizarro C, Tweddell JS, Aortic valve replacement in neonates and infants: an analysis of the Society of Thoracic Surgeons Congenital Heart Surgery Database. J Thorac Cardiovasc Surg 144, 1084–1089 (2012). [PubMed: 22921819]
17. Faza N, Kenny D, Kavinsky C, Amin Z, Heitschmidt M, Hijazi ZM, Single-center comparative outcomes of the Edwards SAPIEN and Medtronic Melody transcatheter heart valves in the pulmonary position. Catheter Cardiovasc Interv 82, E535–541 (2013). [PubMed: 23008193]
18. McElhinney DB, Hellenbrand WE, Zahn EM, Jones TK, Cheatham JP, Lock JE, Vincent JA, Short- and medium-term outcomes after transcatheter pulmonary valve placement in the expanded multicenter US melody valve trial. Circulation 122, 507–516 (2010). [PubMed: 20644013]
19. Berman DP, McElhinney DB, Vincent JA, Hellenbrand WE, Zahn EM, Feasibility and short-term outcomes of percutaneous transcatheter pulmonary valve replacement in small (<30 kg) children with dysfunctional right ventricular outflow tract conduits. Circ Cardiovasc Interv 7, 142–148 (2014). [PubMed: 24569596]
20. Schievano S, Coats L, Migliavacca F, Norman W, Frigiola A, Deanfield J, Bonhoeffer P, Taylor AM, Variations in right ventricular outflow tract morphology following repair of congenital heart disease: implications for percutaneous pulmonary valve implantation. J Cardiovasc Magn Reson 9, 687–695 (2007). [PubMed: 17578725]
21. de Heer LM, Budde RP, Mali WP, de Vos AM, van Herwerden LA, Kluin J, Aortic root dimension changes during systole and diastole: evaluation with ECG-gated multidetector row computed tomography. Int J Cardiovasc Imaging 27, 1195–1204 (2011). [PubMed: 21359833]
22. Kazui T, Izumoto H, Yoshioka K, Kawazoe K, Dynamic morphologic changes in the normal aortic annulus during systole and diastole. J Heart Valve Dis 15, 617–621 (2006). [PubMed: 17044365]
23. Cantinotti M, Giordano R, Scalese M, Murzi B, Assanta N, Spadoni I, Maura C, Marco M, Molinaro S, Kutty S, Iervasi G, Nomograms for two-dimensional echocardiography derived valvular and arterial dimensions in Caucasian children. J Cardiol 69, 208–215 (2017). [PubMed: 27118699]
24. Hammer PE, Roberts EG, Emani SM, Del Nido PJ, Surgical reconstruction of semilunar valves in the growing child: Should we mimic the venous valve? A simulation study. J Thorac Cardiovasc Surg 153, 389–396 (2017). [PubMed: 27665220]
25. Pibarot P, Dumesnil JG, Prosthetic heart valves: selection of the optimal prosthesis and long-term management. Circulation 119, 1034–1048 (2009). [PubMed: 19237674]
26. Sathananthan J, Sellers S, Barlow A, Fraser R, Stanova V, Cheung A, Ye J, Alenezi A, Murdoch DJ, Hensey M, Dvir D, Blanke P, Rieu R, Wood D, Pibarot P, Leipsic J, Webb J, Overexpansion of the SAPIEN 3 Transcatheter Heart Valve: An Ex Vivo Bench Study. JACC Cardiovasc Interv 11, 1696–1705 (2018). [PubMed: 30190060]
27. Rothe CF, Reflex control of veins and vascular capacitance. Physiol Rev 63, 1281–1342 (1983). [PubMed: 6361810]
28. Hainsworth R, Vascular capacitance: its control and importance. Rev Physiol Biochem Pharmacol 105, 101–173 (1986). [PubMed: 3541138]
29. Lurie F, Kistner RL, Eklof B, The mechanism of venous valve closure in normal physiologic conditions. J Vasc Surg 35, 713–717 (2002). [PubMed: 11932668]
30. Vancov G MG, Construction of the Microcirculatory vascular bed in the venous wall. Acta Morph Bulg Acad Sci 5, 20–23 (1984).
31. Franklin KJ, Valves in Veins: An Historical Survey. Proc R Soc Med 21, 1–33 (1927). [PubMed: 19986134]

32. Edwards EA, The Treatment of varicose veins; anatomical factors of ligation of the great saphenous vein. Surgery, Gynecology & Obstetrics 59, 916–928 (1934).
33. Moneta GL, Bedford G, Beach K, Strandness DE, Duplex ultrasound assessment of venous diameters, peak velocities, and flow patterns. J Vasc Surg 8, 286–291 (1988). [PubMed: 3047442]
34. Miyazaki T, Yamagishi M, Maeda Y, Taniguchi S, Fujita S, Hongu H, Yaku H, Long-term outcomes of expanded polytetrafluoroethylene conduits with bulging sinuses and a fan-shaped valve in right ventricular outflow tract reconstruction. J Thorac Cardiovasc Surg 155, 2567–2576 (2018). [PubMed: 29510932]
35. Martin C, Sun W, Simulation of long-term fatigue damage in bioprosthetic heart valves: effects of leaflet and stent elastic properties. Biomech Model Mechanobiol 13, 759–770 (2014). [PubMed: 24092257]
36. Sun W, Abad A, Sacks MS, Simulated bioprosthetic heart valve deformation under quasi-static loading. J Biomech Eng 127, 905–914 (2005); published online EpubNov ([PubMed: 16438226]
37. Vesely I, The evolution of bioprosthetic heart valve design and its impact on durability. Cardiovasc Pathol 12, 277–286 (2003). [PubMed: 14507578]
38. Xuan Y, Krishnan K, Ye J, Dvir D, Guccione JM, Ge L, Tseng EE, Stent and leaflet stresses in a 26-mm first-generation balloon-expandable transcatheter aortic valve. J Thorac Cardiovasc Surg 153, 1065–1073 (2017). [PubMed: 28108064]
39. Lurie F, Kistner RL, Eklof B, Kessler D, Mechanism of venous valve closure and role of the valve in circulation: a new concept. J Vasc Surg 38, 955–961 (2003). [PubMed: 14603200]
40. Nam KH, Yeom E, Ha H, Lee SJ, Velocity field measurements of valvular blood flow in a human superficial vein using high-frequency ultrasound speckle image velocimetry. Int J Cardiovasc Imaging 28, 69–77 (2012).
41. Tibazarwa KB, Volmink JA, Mayosi BM, Incidence of acute rheumatic fever in the world: a systematic review of population-based studies. Heart 94, 1534–1540 (2008). [PubMed: 18669552]
42. O'Byrne ML, Gillespie MJ, Shinohara RT, Dori Y, Rome JJ, Glatz AC, Cost comparison of Transcatheter and Operative Pulmonary Valve Replacement (from the Pediatric Health Information Systems Database). Am J Cardiol 117, 121–126 (2016). [PubMed: 26552510]
43. Geva T, Indications and timing of pulmonary valve replacement after tetralogy of Fallot repair. Semin Thorac Cardiovasc Surg Pediatr Card Surg Annu, 11–22 (2006). [PubMed: 16638542]
44. Murphy JG, Gersh BJ, Mair DD, Fuster V, McGoon MD, Ilstrup DM, McGoon DC, Kirklin JW, Danielson GK, Long-term outcome in patients undergoing surgical repair of tetralogy of Fallot. N Engl J Med 329, 593–599 (1993). [PubMed: 7688102]
45. Nollert G, Fischlein T, Bouterwek S, Bohmer C, Klinner W, Reichart B, Long-term survival in patients with repair of tetralogy of Fallot: 36-year follow-up of 490 survivors of the first year after surgical repair. J Am Coll Cardiol 30, 1374–1383 (1997). [PubMed: 9350942]
46. Buellesfeld L, Stortecky S, Heg D, Gloekler S, Meier B, Wenaweser P, Windecker S, Extent and distribution of calcification of both the aortic annulus and the left ventricular outflow tract predict aortic regurgitation after transcatheter aortic valve replacement. EuroIntervention 10, 732–738 (2014). [PubMed: 25330505]
47. Nakashima M, Watanabe Y, Transcatheter Aortic Valve Implantation in Small Anatomy: Patient Selection and Technical Challenges. Interv Cardiol 13, 66–68 (2018). [PubMed: 29928310]
48. Barbanti M, Yang TH, Rodes Cabau J, Tamburino C, Wood DA, Jilaihawi H, Blanke P, Makkar RR, Latib A, Colombo A, Tarantini G, Raju R, Binder RK, Nguyen G, Freeman M, Ribeiro HB, Kapadia S, Min J, Feuchtner G, Gurtvich R, Alqoofi F, Pelletier M, Ussia GP, Napodano M, de Brito FS Jr., Kodali S, Norgaard BL, Hansson NC, Pache G, Canovas SJ, Zhang H, Leon MB, Webb JG, Leipsic J, Anatomical and procedural features associated with aortic root rupture during balloon-expandable transcatheter aortic valve replacement. Circulation 128, 244–253 (2013). [PubMed: 23748467]
49. Masri A, Schoenhagen P, Svensson L, Kapadia SR, Griffin BP, Tuzcu EM, Desai MY, Dynamic characterization of aortic annulus geometry and morphology with multimodality imaging: predictive value for aortic regurgitation after transcatheter aortic valve replacement. J Thorac Cardiovasc Surg 147, 1847–1854 (2014). [PubMed: 23870156]

50. Yoon SH, Bleiziffer S, De Backer O, Delgado V, Arai T, Ziegelmueller J, Barbanti M, Sharma R, Perlman GY, Khalique OK, Holy EW, Saraf S, Deuschl F, Fujita B, Ruile P, Neumann FJ, Pache G, Takahashi M, Kaneko H, Schmidt T, Ohno Y, Schofer N, Kong WKF, Tay E, Sugiyama D, Kawamori H, Maeno Y, Abramowitz Y, Chakravarty T, Nakamura M, Kuwata S, Yong G, Kao HL, Lee M, Kim HS, Modine T, Wong SC, Bedgoni F, Testa L, Teiger E, Butter C, Ensminger SM, Schaefer U, Dvir D, Blanke P, Leipsic J, Nietlispach F, Abdel-Wahab M, Chevalier B, Tamburino C, Hildick-Smith D, Whisenant BK, Park SJ, Colombo A, Latib A, Kodali SK, Bax JJ, Sondergaard L, Webb JG, Lefevre T, Leon MB, Makkar R, Outcomes in Transcatheter Aortic Valve Replacement for Bicuspid Versus Tricuspid Aortic Valve Stenosis. J Am Coll Cardiol 69, 2579–2589 (2017). [PubMed: 28330793]

51. Yoon SH, Schmidt T, Bleiziffer S, Schofer N, Fiorina C, Munoz-Garcia AJ, Yzeiraj E, Amat-Santos IJ, Tchetche D, Jung C, Fujita B, Mangieri A, Deutsch MA, Ubben T, Deuschl F, Kuwata S, De Biase C, Williams T, Dhoble A, Kim WK, Ferrari E, Barbanti M, Vollema EM, Miceli A, Giannini C, Attizzani GF, Kong WKF, Gutierrez-Ibanes E, Jimenez Diaz VA, Wijeysundera HC, Kaneko H, Chakravarty T, Makar M, Sievert H, Hengstenberg C, Prendergast BD, Vincent F, Abdel-Wahab M, Nombela-Franco L, Silaschi M, Tarantini G, Butter C, Ensminger SM, Hildick-Smith D, Petronio AS, Yin WH, De Marco F, Testa L, Van Mieghem NM, Whisenant BK, Kuck KH, Colombo A, Kar S, Moris C, Delgado V, Maisano F, Nietlispach F, Mack MJ, Schofer J, Schaefer U, Bax JJ, Frerker C, Latib A, Makkar RR, Transcatheter Aortic Valve Replacement in Pure Native Aortic Valve Regurgitation. J Am Coll Cardiol 70, 2752–2763 (2017). [PubMed: 29191323]

52. Helbing WA, Bosch HG, Maliepaard C, Rebergen SA, van der Geest RJ, Hansen B, Ottenkamp J, Reiber JH, de Roos A, Comparison of echocardiographic methods with magnetic resonance imaging for assessment of right ventricular function in children. Am J Cardiol 76, 589–594 (1995). [PubMed: 7677083]

53. Lang RM, Bierig M, Devereux RB, Flachskampf FA, Foster E, Pellikka PA, Picard MH, Roman MJ, Seward J, Shanewise JS, Solomon SD, Spencer KT, Sutton MS, Stewart WJ, Chamber Quantification Writing G, American G Society of Echocardiography's, C. Standards, E. European Association of, Recommendations for chamber quantification: a report from the American Society of Echocardiography's Guidelines and Standards Committee and the Chamber Quantification Writing Group, developed in conjunction with the European Association of Echocardiography, a branch of the European Society of Cardiology. J Am Soc Echocardiogr 18, 1440–1463 (2005). [PubMed: 16376782]

54. Lopez L, Colan SD, Frommelt PC, Ensing GJ, Kendall K, Younoszai AK, Lai WW, Geva T, Recommendations for quantification methods during the performance of a pediatric echocardiogram: a report from the Pediatric Measurements Writing Group of the American Society of Echocardiography Pediatric and Congenital Heart Disease Council. J Am Soc Echocardiogr 23, 465–495; quiz 576-467 (2010). [PubMed: 20451803]

55. Hofferberth SC, Baird CW, Hoganson DM, Quinonez LG, Emani SM, Del Nido PJ, Hammer PE, Mechanical Properties of Autologous Pericardium Change With Fixation Time: Implications for Valve Reconstruction. Semin Thorac Cardiovasc Surg, (2019).

56. Capps SB, Elkins RC, Fronk DM, Body surface area as a predictor of aortic and pulmonary valve diameter. J Thorac Cardiovasc Surg 119, 975–982 (2000). [PubMed: 10788818]

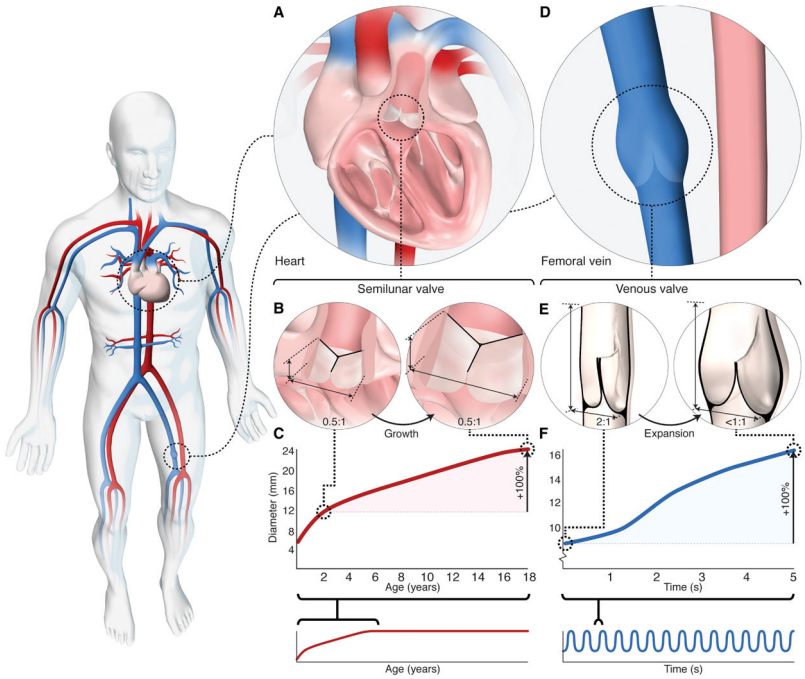

Fig. 1. Geometry and function of human arterial and venous valves.

(A) Schematic depicting arterial semilunar (pulmonary) valve located within the heart. **(B)** Schematic depicting axial height of human semilunar valve relative to annulus diameter. Axial height is ~1/2 the annulus diameter and remains constant with growth. **(C)** Graph of semilunar valve (pulmonary) annulus dimensional change with somatic growth; ~2-fold increase in diameter is observed between the ages of 2 to 18 years in healthy children (graph adapted from reference 23). **(D)** Schematic depicting native venous valve located within vein of lower extremity. **(E)** Schematic depicting leaflet dimensions of human venous valve, at rest (left) and during expansion (right). Axial height is ~2 times the vessel diameter and leaflet contact length (coaptation) is up to half the vessel diameter (30, 31). As the vein expands radially with increased volume load, the venous valve aspect ratio decreases (<1:1) and the sinuses dilate to maintain leaflet contact and ensure unidirectional blood flow. **(F)** Graph of vein diameter in response to large changes in blood volume occurring over a period of seconds. Up to a 4-fold change in vein diameter occurs over a period of seconds (33).

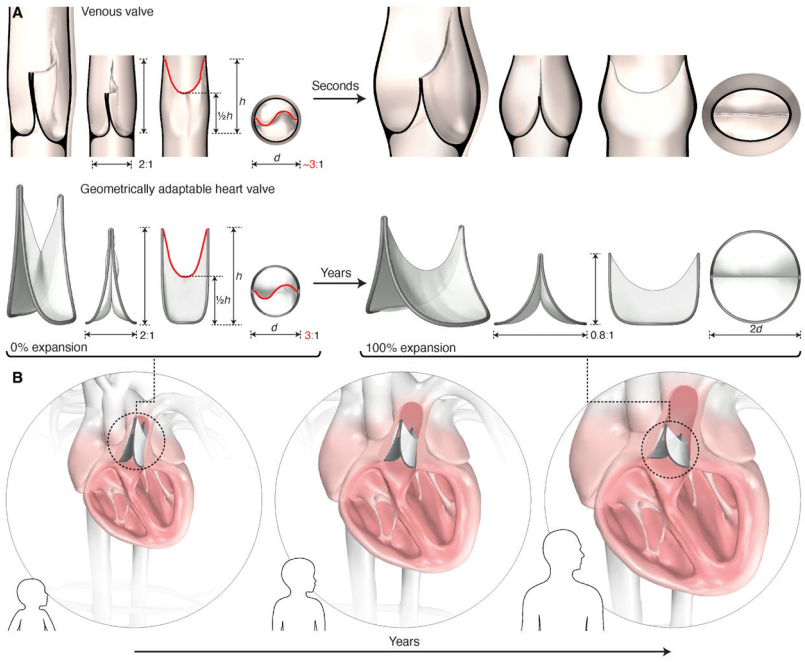

Fig. 2. Design of a biomimetic geometrically adaptable heart valve.

(A) Biomimetic valve design inspired by the geometric profile of the human venous valve. Design is defined by leaflet dimensions, leaflet attachment geometry, and valve expansion geometry. Key leaflet dimensions include the baseline aspect ratio (2:1), leaflet mid-height (1/2h), and free-edge length (red line). The leaflet attachment geometry replicates the 3-dimensional geometric curve created by the venous valve leaflet attachment to the vein wall. The leaflet attachment perimeter is fixed in length, therefore radial expansion is accompanied by a reduction in valve height (aspect ratio decreases to 0.8:1 at 2X expansion; expansion shown on right). **(B)** Schematic representation of the dynamic biomimetic valve geometry as it adapts to the increasing heart dimensions of a growing child via periodic mechanical balloon expansion.

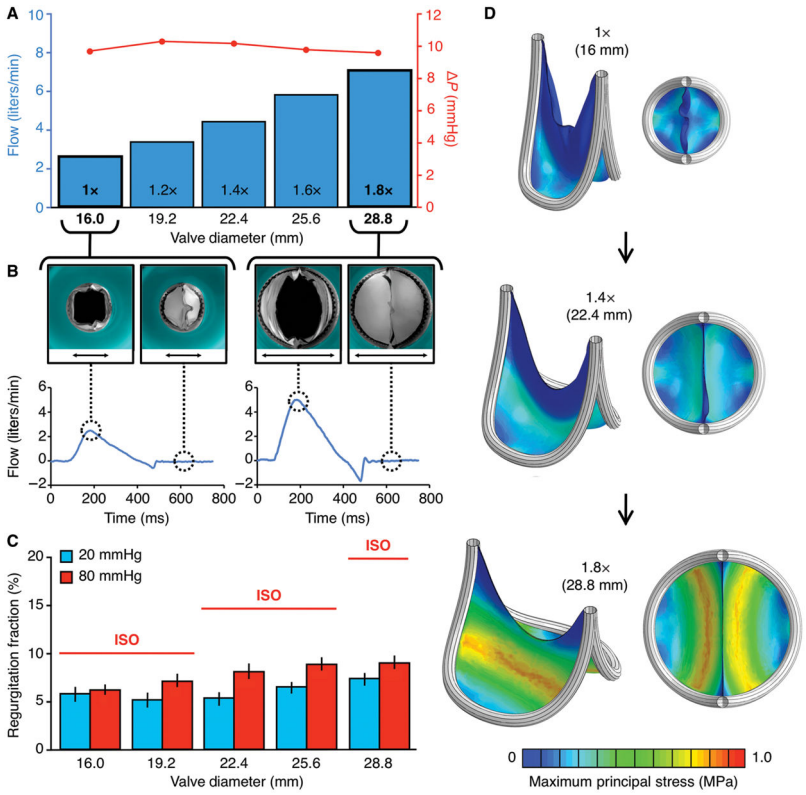

Fig. 3. Flow loop testing and computational modeling of the biomimetic bileaflet valve.

(A-C) Valve prototypes tested at different states of diametric expansion (1X to 1.8X) in an in vitro circulatory flow loop, under physiologic left and right heart conditions. **(A)** Transvalvular (ΔP) pressure gradient (red line) at each stage of valve expansion (1X to 1.8X). Flow adjusted to match valve size and growing child physiology. **(B)** Top view photographs of 1X (black arrow measures 16mm) and 1.8X (black arrow measures 28.8mm) expanded valves within in vitro flow loop system, with leaflets in open (left) and closed (right) position, with their corresponding plots demonstrating flow profiles of the 1X and 1.8X expanded valve geometries. **(C)** Leaflet coaptation (closing function) under right (20 mmHg, blue bars) and left (80 mmHg, red bars) heart loads. Error bars represent ± 1 standard deviation. Red horizontal lines indicate the upper bound industry standard (International Standards Organization; ISO 5840-2:2015) for prosthetic valve regurgitation % under left heart loads. **(D)** Finite element model of leaflet stresses in quasi-static loaded state at 3 different states of valve expansion (1X:16mm ID, 1.4X: 22.4mm ID, 1.8X: 28.8mm ID). Leaflet material is 0.1 mm thickness ePTFE, and the results shown are simulated under right heart (20 mmHg) loads. All plots presented are based on the same scale of maximum principal stress, ranging between 0 to 1 MPa. ID = Internal diameter

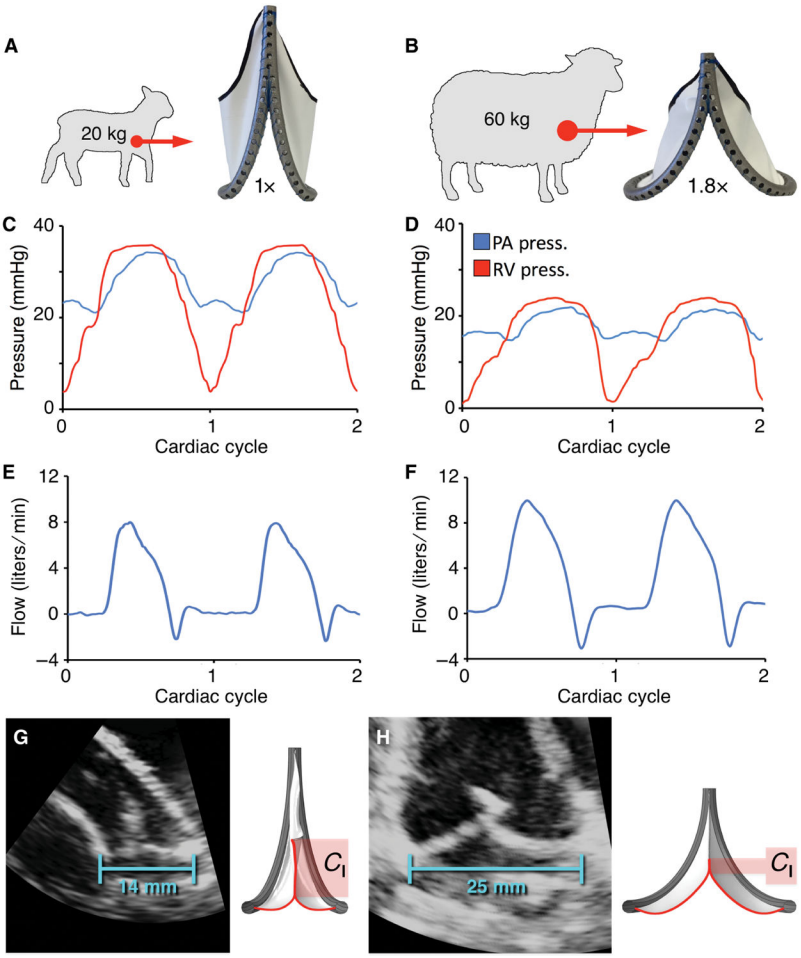

Fig. 4. Acute in vivo validation of primary biomimetic valve function in juvenile and adult sheep.

(A and **B)** Fabricated prototypes implanted at two polar expansion states (1X and 1.8X) in the native pulmonary valve position of juvenile (N = 4) and adult (N = 4) sheep. Representative plots showing right ventricular and pulmonary artery pressures for the **(C)** 1X and (**D)** 1.8X valve geometries. Corresponding pulmonary artery flow for the (**E**) 1X and (**F)** 1.8X valve geometries. Representative echocardiographic images of implanted valves, demonstrating change in coaptation length (C_l) between the (**G**) baseline (1X, 14 mm ID) and (**H)** fully expanded (1.8X, 25 mm ID) geometries. ID = internal diameter.

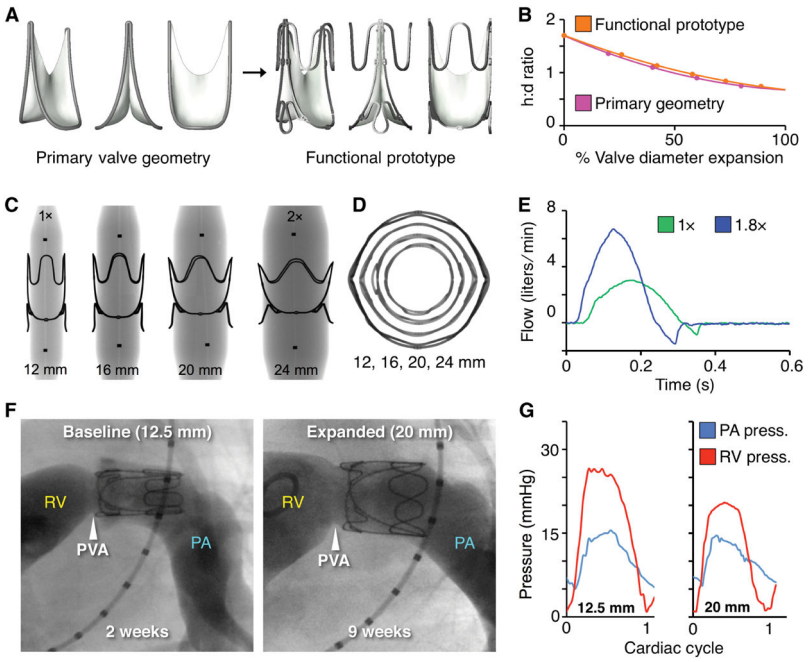

Fig. 5. Functional prototype design and *in vivo* proof-of-concept of valve expansion in a growing lamb model.

(A) CAD models of primary valve geometry and functional prototype containing added structural support features to optimize valve geometry for mechanical expansion. (**B**) Valve expansion geometry (change in aspect ratio with radial expansion) for the primary valve geometry (pink line) and functional prototype (orange line), h:d = height to diameter ratio (**C**) X-ray images of laser-cut stainless-steel functional valve prototypes being expanded via serial balloon dilation. Black dots are x-ray opaque markers on the balloon, denoting zone of constant diameter (**D**) Top-view x-ray transmission images showing geometry of the functional prototype with expansion from 1X to 2X diameter. (**E**) In vitro flow loop testing of functional prototype at two polar expansion states, 1X (green) and 1.8X (blue). Plots show the valve flow cycle at both expansion states. (**F**) Representative right ventricular (RV) angiograms in a lamb showing the expandable biomimetic valve prototype in its baseline (12.5 mm ID) and expanded (20 mm ID, after 3 separate balloon dilation procedures) configuration at 2- and 9-weeks post implantation, respectively. RV = right ventricle, PA = pulmonary artery, PVA = native pulmonary valve annulus (**G**) Representative right ventricular and pulmonary artery pressures recorded at two states of valve expansion, (left:1X, 12.5mm ID) and (right: 1.6X, 20mm ID) at 2 and 9 weeks after implantation.

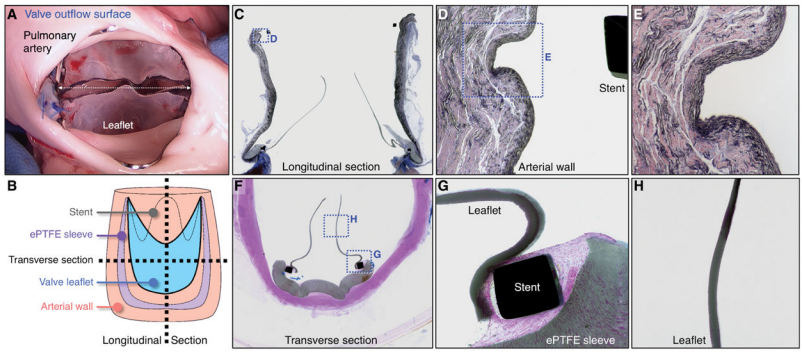

Fig. 6. Macroscopic and histological analysis of biomimetic valve prototype implanted for 10 weeks in a growing lamb.

(A) Representative photograph of valve outflow surface at time of valve explant. White dotted arrow indicates valve internal diameter (20mm). **(B)** Schematic diagram demonstrating method of device sectioning after performing plastic embedding of the explanted specimen (valve and attached pulmonary artery). **(C)** Representative elastin stained longitudinal section of explanted valve specimen (image width = 30 mm). Boxed region shown at higher magnification in (D). **(D)** Higher magnification of native pulmonary artery wall, demonstrating tissue architecture at the site of vessel-stent contact and region of artery wall proximal and distal to vessel-stent interface (image width = 2.5 mm). Boxed region shown at higher magnification in (E). **(E)** Higher magnification of native pulmonary artery wall at site of vessel-stent contact (image width = 1 mm). **(F)** Representative Hematoxylin and Eosin stained transverse section of explanted valve (image width = 20 mm). Boxed regions shown at higher magnification in (G) and (H). **(G)** Higher magnification image of valve leaflet at the site of stent attachment with adjacent ePTFE sleeve (image width = 2.5 mm). **(H)** Higher magnification image showing the mid-section of the valve leaflet (image width = 2.5 mm). All macroscopic and histological images shown are from the same animal. A total of 7 animals received valve implants (See fig. S16, fig. S17).